

## Article

# Experimental Investigation into the Evolution of Probabilistic Characteristics of Early-Age Concrete

Giuseppe Ciaramella Moita , Eduardo M. R. Fairbairn \* , Romildo D. Toledo Filho  and Pierre Rossi

Department of Civil Engineering, Institute for Graduate Studies and Research in Engineering (COPPE), Federal University of Rio de Janeiro, P.O. Box 68506, Rio de Janeiro 21945-970, RJ, Brazil; giuseppe.moita@coc.ufrj.br (G.C.M.); toledo@coc.ufrj.br (R.D.T.F.); p.lupo@yahoo.fr (P.R.)

\* Correspondence: eduardo@coc.ufrj.br

**Abstract:** This paper presents original findings on the heterogeneity of the mechanical properties of concrete of an early age, dependent on the evolution of the hydration reaction. The properties investigated are the compressive strength, the Young's modulus, and the flexural tensile strength. To achieve this, we employed a testing apparatus in which the samples underwent curing in a chamber that followed the same temperature profile as an adiabatic calorimeter. This method enabled us to monitor the hydration progress across multiple samples. We used a function derived from the literature, with specific adaptations, to model the evolution of normalized properties in relation to hydration. Heterogeneity was quantified through the use of the dispersion coefficient. The key finding of this study is that the dispersion coefficient for the analyzed mechanical properties diminishes with the advancement of hydration, until reaching a specific threshold. Beyond this point, the impact of microcracking on the various properties becomes increasingly pronounced, varying according to the particular property being examined. Moreover, this paper presents initial functions designed to offer formulas that assist in modeling concrete within probabilistic numerical simulations from the early stages of its development.

**Keywords:** hydration; concrete; heterogeneity; early age



**Citation:** Moita, G.C.; Fairbairn, E.M.R.; Toledo Filho, R.D.; Rossi, P. Experimental Investigation into the Evolution of Probabilistic Characteristics of Early-Age Concrete. *Buildings* **2024**, *14*, 668. <https://doi.org/10.3390/buildings14030668>

Academic Editors: Giuseppina Uva, Nicoleta Cobirzan and Radu Muntean

Received: 19 January 2024  
Revised: 21 February 2024  
Accepted: 26 February 2024  
Published: 2 March 2024



**Copyright:** © 2024 by the authors. Licensee MDPI, Basel, Switzerland. This article is an open access article distributed under the terms and conditions of the Creative Commons Attribution (CC BY) license (<https://creativecommons.org/licenses/by/4.0/>).

## 1. Introduction

Over the past five decades, probabilistic models for numerical simulations of concrete have attracted significant attention from various researchers seeking more realistic methods to simulate structural behavior in distinct ways. Shinozuka introduced an early probabilistic model compatible with finite element analysis, taking into account the spatial variation of concrete strength to capture statistical size effects [1]. Van Mier et al., developed a lattice model within a three-phase particle composite structure similar to concrete [2]. Benkemoun et al., created a mesoscale model for failure representation using 3D finite elements with embedded discontinuities [3]. Tang et al. incorporated concrete heterogeneity using the Weibull distribution law and a mesoscale mesh of finite elements [4]. Sellier and Millard addressed the random nature of tensile strength, along with softening behavior, through a variant of the Weibull theory. In this variant, the classical weakest link theory was reformulated in a non-local form, allowing for a second gradient implementation [5].

In this paper, special focus is placed on the probabilistic cracking model (PCM), which has been under development at IFSTTAR (formerly LCPC) since 1987. Initially proposed by Rossi [6] and subsequently refined by Tailhan et al. [7], this model has been extended to encompass reinforced concrete [8], fiber-reinforced [9], concrete cracking [10] and ultra-high-performance fibre-reinforced concrete (UHPFRC) [11]. It has been the subject of extensive collaboration between Gustave Eiffel University (formerly LCPC) and COPPE (Federal University of Rio de Janeiro) since the early 1990s, with advancements in probabilistic finite elements analysis [12], inverse analysis, and artificial neural networks [13] combined with computational optimization.

The PCM contributes to a more realistic structural design, offering economic and sustainability advantages through the dual effect of utilizing materials at their maximum efficiency and enhancing their durability. In this context, since 2012 in Aix-en-Provence, studies employing PCM have featured prominently among the flagships at the Numerical Modeling Strategies for Sustainable Concrete Structures (SSCSs) conferences [14].

The PCM characterizes the behavior of concrete based on two fundamental attributes: heterogeneity and sensitivity to scale effects [15]. It has been thoroughly validated for structures subjected to quasi-static loads and for mature concrete no longer of an early age. Here, we adopt the definition from the RILEM TC-254 State of the Art Report [16] that considers early-age concrete as that in the period following the percolation threshold, characterized by rapid changes in material properties influenced by hydration. The underlying principles of PCM can be summarized as follows: (i) concrete's heterogeneity stems from its composition, with local mechanical properties such as tensile strength ( $f_{ct}$ ) and shear strength ( $\tau_c$ ) being randomly distributed; (ii) scale effects arise from material heterogeneity, meaning that the mechanical response is directly influenced by the volume of material under stress; (iii) the cracking process is governed by defects in the cement paste, material heterogeneity, and the development of tensile stress gradients. The model is formulated within the framework of the finite element method and incorporates the following physical considerations [7,8]: (i) each element corresponds to a specific volume of heterogeneous material; (ii) the tensile strength is stochastically distributed across all elements of the mesh using a Weibull distribution function, the parameters of which are contingent upon the ratio between the volume of the finite element and the volume of the largest aggregate, as well as the compressive strength, which serves as a reliable indicator of the quality of the cement paste. It is important to note that concrete is treated in the PCM as linear elastic within volume elements, while cracks are represented using interface elements with a fully brittle constitutive relationship. Consequently, at the elemental level, tensile strength becomes a probabilistic variable, and fracture energy remains unaccounted for. Macroscopic tensile strength and crack energy emerge as structural properties reliant on the sample or structure size, as demonstrated in [12]. This way, the size effect on macroscopic tensile strength ( $f_{ct}$ ) and specific fracture energy ( $G_f$ ) manifests in the PCM as macroscopic properties that are dependent on the size of the analyzed structure, as experimentally verified. Rossi et al. studied the size effect of  $f_{ct}$  in direct tension tests for specimens with diameters ranging from 20 mm to 300 mm and a slenderness ratio of 2 [15]. Bazant and Kazemi [17] and Wittmann et al. [18] analyzed the size effect on  $G_f$  obtained via the RILEM three-point bending test. Therefore, this paper does not explore the specific fracture energy ( $G_f$ ) in terms of its variability with hydration. A comprehensive examination of the evolution of  $G_f$  during the early stages is available in the recent RILEM State of the Art Report [16], which reveals only a limited number of references addressing this topic. Notably, the formulas suggested by De Schutter and Taerwe [19] for concretes with a degree of reaction exceeding 0.8 are highlighted. Another formulation, proposed by Bassam et al. [20], considers the thermo-activation phenomenon based on the maturity concept, finding support in references [21,22].

When the focus shifts to analyzing the cracking process during the early age of the concrete, additional parameters are required to characterize the material's heterogeneity. While the development of concrete properties in relation to the hydration reaction during its early age has been extensively studied [16,19,23,24], there is a notable absence of references regarding the evolution of the variability of the properties that are essential for probabilistic models, such as compressive and tensile strengths.

To address this knowledge gap, an experimental study was conducted to investigate the evolution of heterogeneity in compressive strength, Young's modulus, and flexural tensile strength during the early stages of hydration. The findings revealed that the dispersion coefficient of these mechanical properties diminished as hydration progressed. This suggests that, during its early age, the structure of hardened concrete exhibits greater heterogeneity compared with more advanced stages of hydration.

## 2. Materials

### 2.1. Cement

Portland cement with slag, or CII-E, was employed in accordance with the specifications outlined in the National Brazilian Standard (NBR) 16697 [25]. Its main nominal contents (in mass) consisted of clinker (0.51–0.94), slag (0.06–0.34), and filler (0–0.15). To ensure consistency in its properties, all the cement utilized in this study originated from the same batch. Its main physical, chemical, and mechanical characteristics are presented in Table 1. Specific gravity and compressive strength data were obtained from the NBR 16605 and NBR 7215 standards, respectively [26,27].

**Table 1.** Physical and chemical properties of the Portland cement.

|                              |                                |        |
|------------------------------|--------------------------------|--------|
| Compressive strength (MPa)   | 1 day                          | 11.87  |
|                              | 3 days                         | 24.25  |
|                              | 7 days                         | 37.23  |
|                              | 28 days                        | 56.12  |
| Chemical composition (%)     | CaO                            | 55.73  |
|                              | SiO <sub>2</sub>               | 21.43  |
|                              | Al <sub>2</sub> O <sub>3</sub> | 6.03   |
|                              | SO <sub>3</sub>                | 3.89   |
|                              | MgO                            | 2.39   |
|                              | Fe <sub>x</sub> O <sub>y</sub> | 2.13   |
|                              | K <sub>2</sub> O               | 0.98   |
|                              | Na <sub>2</sub> O              | 0.47   |
|                              | Others                         | 0.91   |
|                              | Loss on ignition               | 6.04   |
| Actual packing density *     |                                | 0.5679 |
| Density (g/cm <sup>3</sup> ) |                                | 3.118  |

\* As defined by de Larrard [28].

### 2.2. Aggregates

The fine aggregates consisted of natural sand, with a nominal diameter less than 4.75 mm. The coarse aggregates were composed of granite-type stones, with a nominal diameter ranging from 4.75 mm to 9.5 mm. Prior to their characterization and incorporation into the concrete, the aggregates were homogenized and appropriately stored. The aggregates were also all from the same batch.

The main characteristics of the aggregates are presented in Table 2, and their granular distribution is represented in Figure 1. The specific mass of the area and that of the gravel were determined following the Brazilian standards NBR NM 52 and NBR NM 53 [29,30] and the water absorption was determined in accordance with NBR NM 30 and NBR NM 53 [30,31], respectively. The parameters  $p$  and  $q$  were determined in accordance with the CPM [28] and the granulometry was obtained through the standard NBR NM 248 [32].

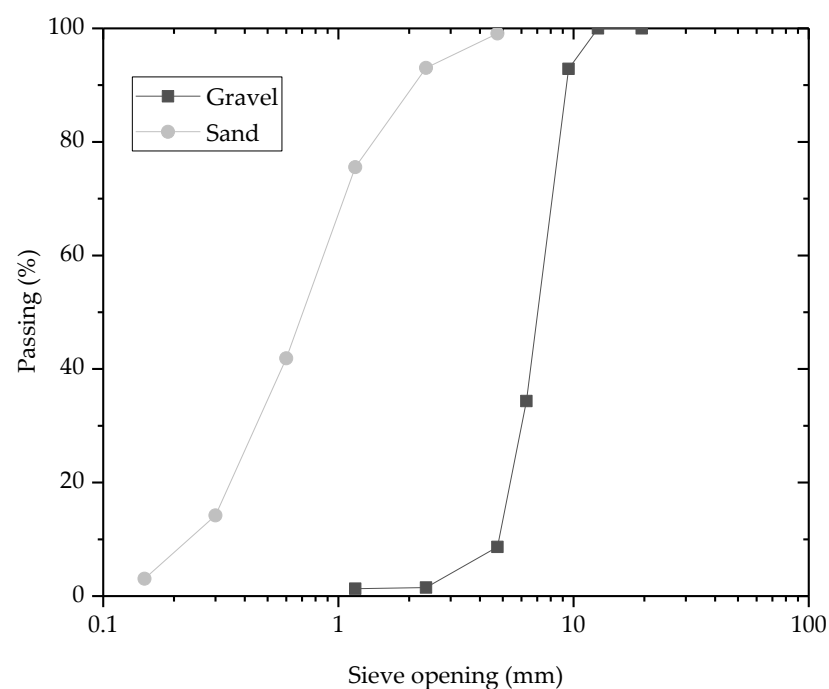
### 2.3. Concrete

A standard 40 MPa compressive strength concrete was employed, comprising cement, gravel, and sand, without the utilization of superplasticizer. The mix design was developed in accordance with De Larrard's [28] compressible packing model (CPM), using the software Bétonlab Pro 3 [33]. The mixture proportions are given in Table 3.

**Table 2.** Physical and mechanical properties of fine and coarse aggregates.

| Properties                   | Fine Aggregate (Sand)  | Coarse Aggregate (Gravel) |
|------------------------------|------------------------|---------------------------|
| Maximum grain size (mm)      | 4.75                   | 9.52                      |
| Density (g/cm <sup>3</sup> ) | 2.37                   | 2.87                      |
| Water absorption rate (%)    | 0.74                   | 1.39                      |
| Actual packing density *     | 0.7451                 | 0.6347                    |
| CPM parameter *              | P                      | -                         |
|                              | q (MPa <sup>-1</sup> ) | -                         |

\* As defined by de Larrard [28].

**Figure 1.** Granulometry of fine and coarse aggregates.**Table 3.** Concrete mix design.

| Components       | Content                |
|------------------|------------------------|
| Coarse aggregate | 1169 kg/m <sup>3</sup> |
| Fine aggregate   | 519 kg/m <sup>3</sup>  |
| Cement           | 550 kg/m <sup>3</sup>  |
| Water            | 210 kg/m <sup>3</sup>  |
| w/c ratio        | 0.38                   |

To avoid introducing heterogeneity in the mechanical properties due to variations in raw materials, we ensured that both the cement and aggregates were consistently sourced from the same batches. Conversely, we produced concrete through multiple pours without attempting to eliminate pour-related heterogeneity, aiming to maintain realism. This approach reflects the reality that the construction of an actual structure involves several pouring stages. Therefore, the normalized individual results of mechanical properties do not directly correspond to specific pours. Additionally, clusters that gather individual

results of mechanical properties (see Section 3.5) are not linked to specific pours; instead, they are categorized based on certain values of the degree of heat development.

### 3. Experimental Methods

#### 3.1. Coupled Calorimetry/Cure Chamber

Among the various methods available for assessing concrete's hydration evolution [16], we chose adiabatic calorimetry for its capacity to continuously measure heat development, thereby reflecting hydration evolution. Additionally, by regulating the temperature of the curing chamber to match that of the adiabatic calorimeter, we ensured that the samples in the chamber shared the same hydration history as those inside the calorimeter. Hence, the microstructural properties of the samples in the curing chamber, including porosity, can be assumed to mirror those of the samples inside the calorimeter.

The adiabatic calorimeter comprised a 2 L concrete sample immersed in a constantly circulating water bath. Initially, both the water and concrete were in thermal equilibrium. As the temperature of the concrete sample increased by 0.1 °C due to the exothermic reactions, the water bath's temperature increased via electrical resistors controlled by an electronic control unit. This method ensured that the water temperature matched that of the concrete sample throughout the hydration reaction. Figure 2 presents a schematic representation of the adiabatic calorimeter, along with a photograph of the specific apparatus utilized in this study.

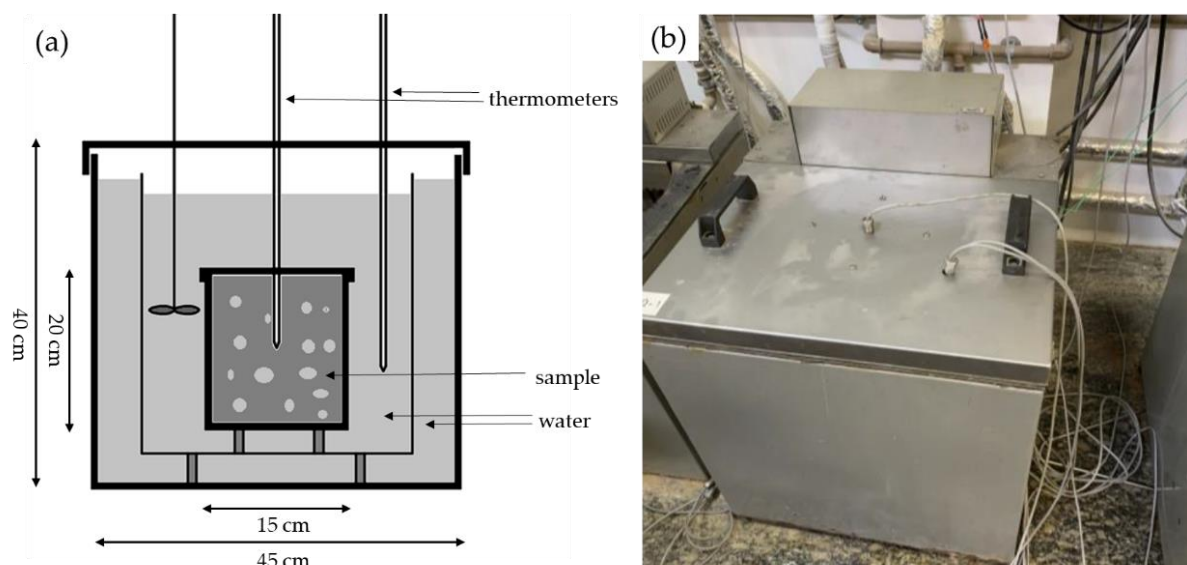


**Figure 2.** Adiabatic calorimeter (a) sketch; (b) photography.

In the mixing process, first, the coarse and fine aggregates were mixed with approximately one-third of the water for 30 s in a concrete mixer. Next, the cement was added to the mixture along with an additional one-third of the total water, and mixing continued for another 30 s in the concrete mixer. Finally, the remaining water was added, and the concrete was mixed for an additional 5 min until achieving homogeneity.

After mixing, the concrete was introduced into the inner chamber of the adiabatic calorimeter. A thin layer of expanded polystyrene previously immersed in oil was utilized to line the chamber, facilitating the subsequent removal process. A robust plastic bag was positioned within the sheet, to contain the concrete. The pouring procedure was conducted in two stages. Initially, a layer weighing 2 kg was deposited and subjected to 30 s of vibration, followed by an additional layer weighing 1.74 kg that underwent an additional 30 s of vibration.

At the end of the vibration, a sealed iron tube was positioned at the center of the concrete mass. A thermometer was inserted into this iron tube, which had previously been

filled with oil to enhance the conduction of the heat released by the concrete. Subsequent to the initial temperature measurement of the concrete, the water temperature was adjusted to match that of the material by incorporating either cold or hot water. This adjustment was made to prevent any interference with the thermal activation of the concrete. The thermometers had a sensitivity of 0.1 °C and acquired the temperature of both the water and the samples throughout the duration of the test. The temperature readings were recorded every minute for the purpose of constructing the temperature graph.

The aim was to perform mechanical tests on concrete with different known hydration histories in its early stages. To achieve this, a temperature-regulated water chamber was integrated with the adiabatic calorimeter. The chamber was equipped with a controller that synchronized its water temperature with that of the outer chamber bath of the adiabatic calorimeter. Consequently, the specimens within the curing chamber experienced an identical temperature profile and, therefore, the same hydration history as the specimen within the calorimeter. Figure 3 provides a schematic illustration of this process.

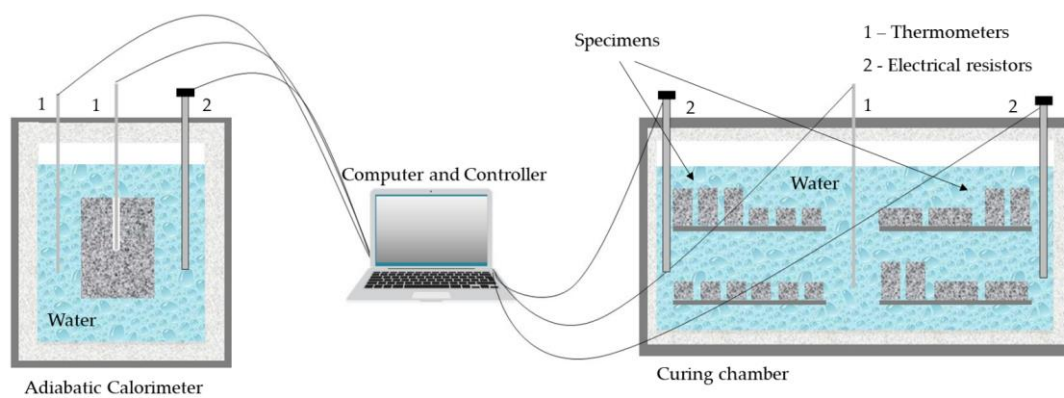


**Figure 3.** Sketch of adiabatic calorimeter and cure chamber.

To prevent leaching, a water-resistant marine grease was applied to all the specimens, and the top of the mold was covered with a layer of plastic film, which was then secured in place using masking tape, as illustrated in Figure 4. In this process, we aimed to realistically simulate conventional concrete curing and operational conditions.

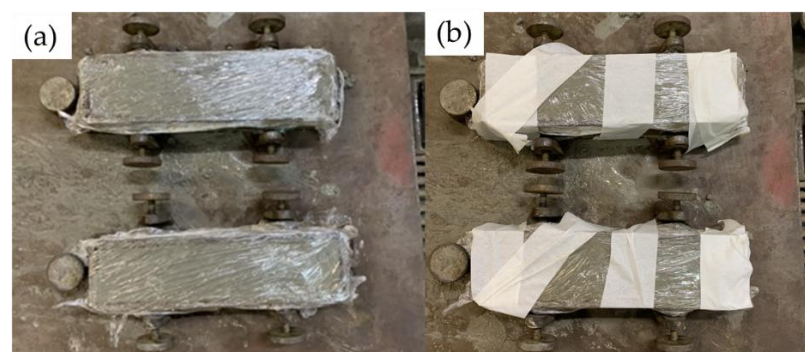


**Figure 4.** Coating of the specimens with (a) plastic film and (b) masking tape.

Within the framework of the experiments outlined in this paper, the degree of heat development ( $\alpha^Q$ ) described by Fairbairn and Azenha [16] was used to characterize the progression of the hydration reaction in the early stages until the stabilization of the measurements within the adiabatic calorimeter:

$$\alpha^Q(t) = \frac{Q(t)}{Q_{max}} = \frac{\Delta T_{ad}(t)}{\Delta T_{ad,max}} \quad (1)$$

In Equation (1),  $Q(t)$  and  $\Delta T_{ad}(t)$  are, respectively, the heat of the hydration released and the adiabatic temperature at a time  $t$ .  $Q_{max}$  is the total heat of the hydration measured by the calorimeter and  $\Delta T_{ad,max}$  is the adiabatic temperature corresponding to the end of the calorimetric test when variations of  $\Delta T_{ad}(t)$  are no longer measured within the sensitivity limits of the calorimeter.

Although the temperatures within the adiabatic experiments ceased to vary after 90 h, the experiment was extended for 7 days. Then, the specimens were removed from the curing chamber at different temperatures  $\Delta T_{ad}(t)$  for mechanical tests to be performed following several degrees of heat development.

We employed the normalized parameter  $\alpha^Q$  as a measure of hydration evolution during the early stages, alongside normalized values of mechanical properties. This approach allowed us to establish relationships between these parameters in the early stages, independent of the concrete mixes. This method aligns with the consensus reported in various references, such as [16,34].

### 3.2. Compression Tests

The compression tests were carried out on cylindrical specimens of 75 mm diameter and 150 mm height, using a 1000 kN Shimadzu testing machine with an axial displacement rate of 0.3 mm/min. The Young's modulus was measured with two 5 mm LVDTs positioned on opposing sides of a 10 cm length support centrally positioned within the cylinder. In the test for  $\Delta T_{ad,max}$ , 18 specimens were used, chosen for the normalization of results. For other values of  $\Delta T_{ad}(t)$ , between 6 and 13 specimens were employed.

### 3.3. Bending Tests

The flexural tensile strength ( $f_t$ ) was determined using 4-point bending tests conducted on  $50 \times 50 \times 230$  mm beams.

The span length ( $L$ ) was 160 mm, and two loads ( $P$ ) were applied via two rollers at a distance of  $c = 50$  mm from the supports. The tests were carried out using a 100 kN Shimadzu universal machine with a deflection rate of 0.3 mm/min, applied to the center of the lower face of the specimen. The flexural tensile strength  $f_t$  (MPa) was calculated in the usual way using the following relationship:

$$f_t = \frac{6(P_{max} \cdot c)}{bh^2} \quad (2)$$

where  $P_{max}(N)$  is the maximum load reached by the beam,  $b = h = 50$  mm.

In the test for  $\Delta T_{ad,max}$ , 13 specimens were used, chosen for the normalization of results. For other values of  $\Delta T_{ad}(t)$ , between 5 and 6 specimens were employed.

### 3.4. Ultrasonic Pulse Measurement

The percolation threshold, which signifies the point when the cementitious material transitions into a solid state, was identified via the ultrasonic pulse measurement method, using an ultrasonic cement analyzer (UCA). A 5265 SGSA UCA model of the Chandler Engineering brand was used. The test was programmed to maintain a temperature of 23.5 °C and a pressure of 1 atm over a duration of one week. The percolation threshold was defined in accordance with the methodology established by Rocha [35]. According to the author, the timing of the percolation threshold is calculated at the moment when the ultrasonic speed presents a significant increase due to the appearance of a crystalline structure in the concrete.

### 3.5. Statistical Analysis

The heterogeneity of the compressive strength ( $f_c$ ), the Young's modulus ( $E_c$ ), and the flexural tensile strength ( $f_t$ ) were analyzed. These properties are generically named as

$\Pi_p \in \{f_c, E_c, f_t\}$ . To ensure consistency in the analyses, they were normalized with respect to the mean values obtained for a degree of heat development equal to 1:

$$\bar{\Pi}_{p,i}(\alpha^Q) = \frac{\Pi_{p,i}(\alpha^Q)}{\Pi_{p,\mu}(1)} \quad (3)$$

$$\Pi_{p,\mu}(1) = \frac{\sum_{i=1}^{nsp1} \Pi_{p,i}(1)}{nsp1} \quad (4)$$

where  $i$  represents an individual sample,  $\mu$  stands for mean,  $nsp1$  is the number of samples of property  $\Pi_p$  that has the degree of heat development  $\alpha^Q = 1$ .

The analysis of the mechanical tests was conducted in two phases. At first, the function  $\bar{\Pi}_p(\alpha^Q)$  was fitted to the experimental values. Subsequently, for a given property  $\Pi_p$ , samples were classified within clusters generically denominated as  $cl_{p,kcl}$ , where  $kcl$  is the number of the cluster, defined for values of  $\alpha^Q$  within the range  $\alpha_{p,kcl,inf}^Q \leq \alpha_{p,kcl,i}^Q \leq \alpha_{p,kcl,sup}^Q$ . Here,  $\alpha_{p,kcl,i}^Q$  represents a generic  $i$  value of  $\alpha^Q$  of the property  $p$  for the cluster numbered  $kcl$  of this property, while  $inf$  and  $sup$  indexes are the lower and upper values of  $\alpha^Q$  for this cluster. The clusters were selected to be as narrow as possible while ensuring an adequate number of samples, thereby allowing meaningful statistical analysis. Therefore, a generic cluster  $cl_{p,kcl}$  with  $n_{p,kcl}$  samples encompasses the degrees of heat development  $\alpha_{p,kcl,i}^Q$ ,  $i = 1, n_{p,kcl}$ , having the mean degree of heat development:

$$\alpha_{p,kcl,\mu}^Q = \frac{\sum_{i=1}^{n_{p,kcl}} \alpha_{p,kcl,i}^Q}{n_{p,kcl}} \quad (5)$$

For all normalized properties and for each cluster, the mean ( $\bar{\Pi}_{p,kcl,\mu}$ ), the standard deviation ( $\bar{\Pi}_{p,kcl,\sigma}$ ), and the dispersion coefficient ( $\bar{\Pi}_{p,kcl,v}$ ) were determined via the following expressions:

$$\bar{\Pi}_{p,kcl,\mu} = \frac{\sum_{i=1}^{n_{p,kcl}} \bar{\Pi}_{p,kcl,i}}{n_{p,kcl}} \quad (6)$$

$$\bar{\Pi}_{p,kcl,\sigma} = \sqrt{\frac{1}{(n_{p,kcl} - 1)} \sum_{i=1}^{n_{p,kcl}} (\bar{\Pi}_{p,kcl,i} - \bar{\Pi}_{p,kcl,\mu})^2} \quad (7)$$

$$\bar{\Pi}_{p,kcl,v} = \frac{\bar{\Pi}_{p,kcl,\sigma}}{\bar{\Pi}_{p,kcl,\mu}} \quad (8)$$

Although the standard deviation was presented for several clusters, the dispersion coefficient was chosen as the primary parameter to characterize the heterogeneity of a cluster, given its consideration of the extent of variability concerning the mean of the cluster population.

It is important to note that for clusters with a mean degree of heat development equal to 1, the standard deviation is equivalent to the coefficient of variation, as expected, given that the mean value of the normalized properties for  $\alpha^Q = 1$  is  $\bar{\Pi}_{p,\mu}(1) = 1$ .

## 4. Results and Discussion

### 4.1. Adiabatic Temperature Rise

Initial temperatures of the calorimetric tests, as well as the curing process, were used within the range of 15 °C to 25 °C to ensure the same  $\alpha^Q$  values despite different temperature histories. Figure 5 shows the adiabatic temperature rise in a semi-log scale for some typical tests. These curves illustrate that, as anticipated, the magnitudes of the

temperature rises were nearly identical, differing by only 5% across the different tests. Furthermore, the results highlight the well-established thermo-activation phenomenon.

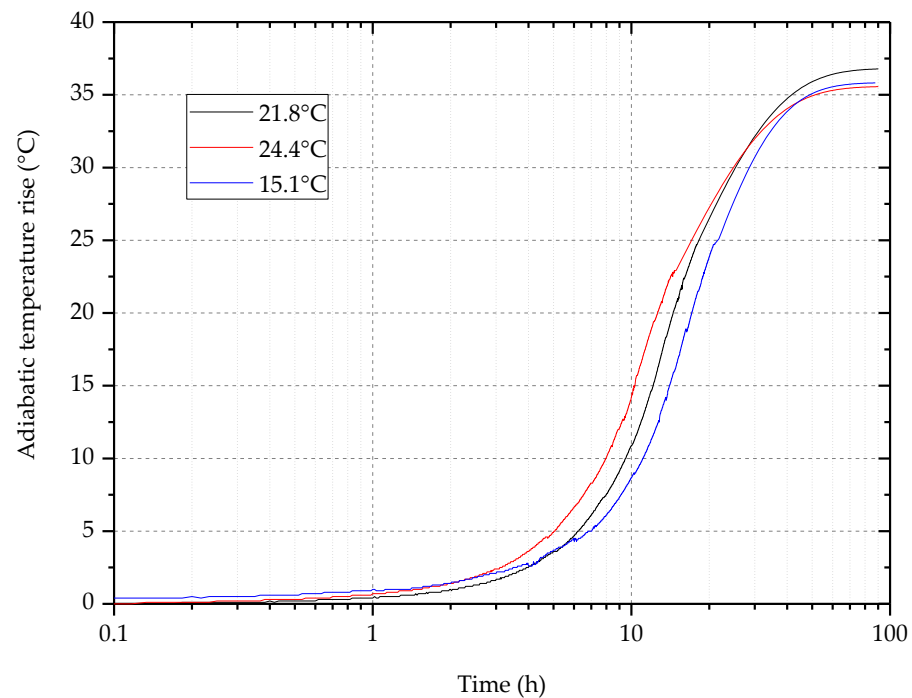


**Figure 5.** Adiabatic temperature rise for different initial temperatures (log scale).

The temperatures measured in the curing chamber corresponded to those in the calorimeter. Therefore, by using Equation (1), it is possible to determine the degree of heat development at any time of the adiabatic experiment provided that  $\Delta T_{ad,max}$  is known. Given the impracticality of conducting mechanical tests for numerous samples at precisely the same  $\alpha^Q$ , it was decided to create clusters gathering samples that can be reported to a single averaged degree of heat development. This concept is further elucidated in the subsequent analysis of the results detailed in the following paragraphs.

#### 4.2. Evolution of the Properties with the Degree of Heat Development

Figures 6–8 present the progression of the normalized properties, specifically the compressive strength  $\bar{f}_c(\alpha^Q)$ , Young's modulus  $\bar{E}_c(\alpha^Q)$ , and flexural tensile strength  $\bar{f}_t(\alpha^Q)$ , generically named  $\bar{\Pi}_p$ , as described in Section 3.5. This normalization was performed by dividing the individual values of the properties ( $\bar{\Pi}_p$ ) by the average for the degree of heat development  $\bar{\Pi}_p(1)$ , given by Formula (4). The average values of compressive strength, tensile strength, and Young's modulus for a degree of heat development equal to 1 are, respectively, 34.3 MPa, 4.04 MPa, and 22.38 GPa. The patterns of the evolution of these properties with the degree of heat development are similar to those in other studies presented in the literature (see, for instance, the several models presented by Fairbairn and Azenha [16]): the compressive strength is concave downward, the flexural tensile strength is practically linear, and the Young's modulus is lightly concave upward [36]. The results were adjusted with twofold models, considering the absence of mechanical properties prior to the percolation threshold, which denotes the specific degree of heat development ( $\alpha_0^Q$ ) when the material becomes solid. Consequently, following an initial set of values fitted with

a straight line, the subsequent values are represented by a non-linear function, as presented by Kraus and Hariri [24] and used by Fairbairn et al. [37] with some minor adaptations.

$$\bar{\Pi}_p(\alpha) = \begin{cases} a_p (\alpha^Q - \alpha_0^Q) & \text{for } \alpha_0^Q \leq \alpha^Q \leq \alpha_{a,p}^Q \\ \left(\frac{\alpha^Q - \kappa}{1 - \kappa}\right)^{n_{ip}} & \text{for } \alpha_{a,p}^Q < \alpha^Q \leq 1 \end{cases} \quad (9)$$

$$a_p = \frac{1}{(\alpha_{a,p}^Q - \alpha_0^Q)} \left(\frac{\alpha_{a,p}^Q - \kappa}{1 - \kappa}\right)^{n_p}$$

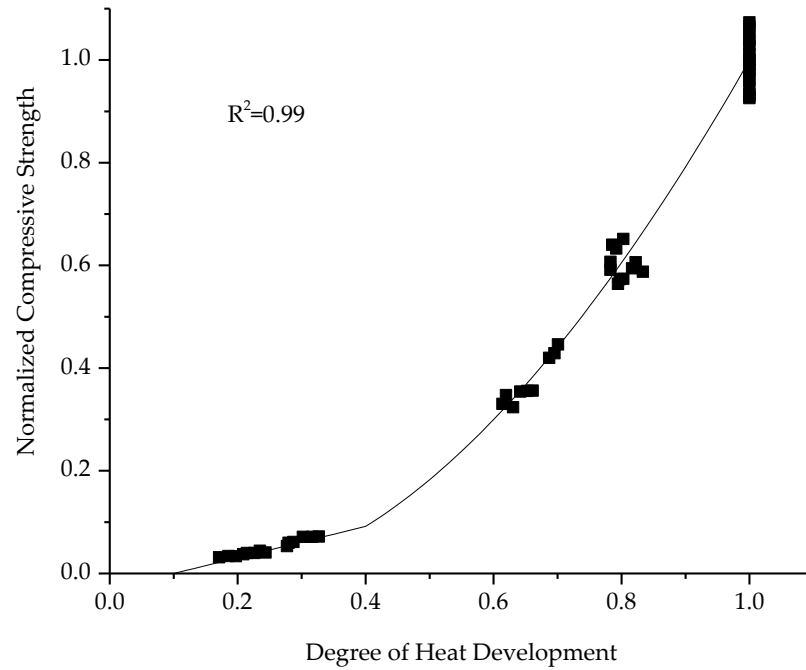


Figure 6. Normalized compressive strength versus  $\alpha^Q$ .

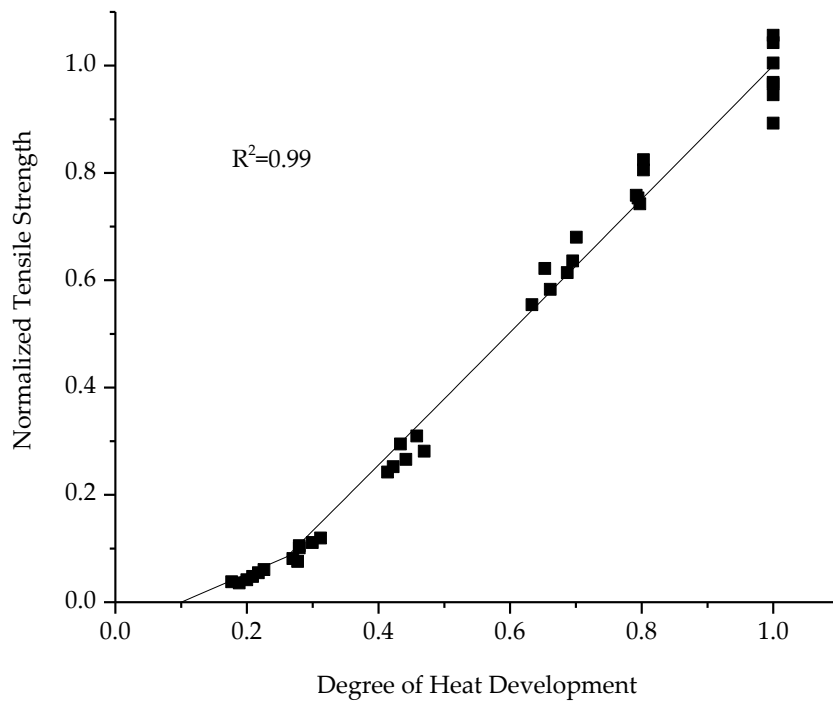
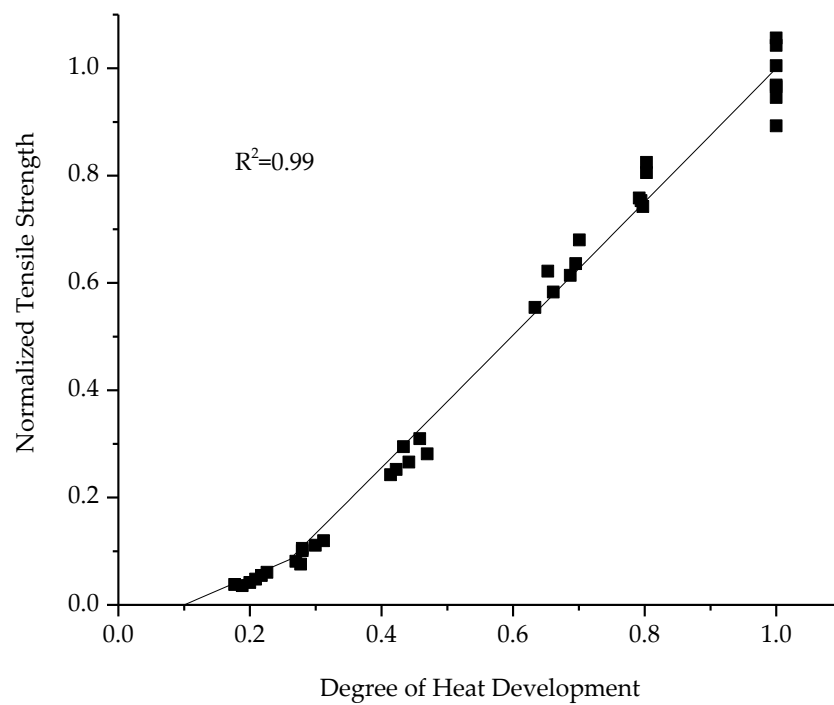


Figure 7. Normalized Young's modulus versus  $\alpha^Q$ .



**Figure 8.** Normalized flexural tensile strength versus  $\alpha^Q$ .

In Equation (9), the values  $n_p \in \{1.77, 0.90, 1.01\}$ ,  $\alpha_{a,p}^Q \in \{0.40, 0.27, 0.26\}$ ,  $\kappa = 0.19$  were used; the value of  $\alpha_0^Q = 0.08$  was approximated based on a UCA test carried out in a  $w/c = 0.38$  cement paste produced with the same cement as used in the present research, and described in part 3.4. These curves have the coefficient of determination  $R_p^2 \in \{0.99, 0.95, 0.99\}$ .

#### 4.3. Statistical Analysis of Compressive Strength and Young's Modulus

Given that the compressive strength tests and the Young's modulus tests were conducted on the same samples and at the same time, virtually identical clusters (as defined in Section 3.5) were employed for both properties. An exception was made for the first cluster because the modulus of elasticity for low values of  $\alpha^Q$  could not be determined, due to experimental difficulties. In this way, the samples were gathered for analysis of the compression tests within 4 clusters, as presented in Table 4, where the main statistical indicators are also presented. For each cluster, the curing state of the sample group is indicated by the average  $\alpha^Q$ , reflecting the mean hydration development of the samples associated with that particular cluster. The standard deviation had an evolution trend contrary to the dispersion coefficient, highlighting the importance of characterizing the heterogeneity of the cluster relative to the mean value of the property within the cluster.

**Table 4.** Results for compressive strength and Young's modulus.

| $cl_{kcl}$ | $\alpha_{kcl,inf} - \alpha_{kcl,sup}$ | $\alpha_{kcl,\mu}^Q$ | $\bar{f}_{c,kcl,\mu}$ | $\bar{f}_{c,kcl,\sigma}$ | $\bar{f}_{c,kcl,v}$ | $\bar{E}_{c,kcl,\mu}$ | $\bar{E}_{c,kcl,\sigma}$ | $\bar{E}_{c,kcl,v}$ |
|------------|---------------------------------------|----------------------|-----------------------|--------------------------|---------------------|-----------------------|--------------------------|---------------------|
| 1a         | 0.15 – 0.35                           | 0.25                 | 0.05                  | 0.015                    | 0.306               | -                     | -                        | -                   |
| 1b         | 0.25 – 0.35                           | 0.30                 | -                     | -                        | -                   | 0.11                  | 0.070                    | 0.65                |
| 2          | 0.60 – 0.70                           | 0.66                 | 0.37                  | 0.045                    | 0.122               | 0.63                  | 0.088                    | 0.139               |
| 3          | 0.75 – 0.85                           | 0.8                  | 0.60                  | 0.029                    | 0.048               | 0.78                  | 0.073                    | 0.093               |
| 4          | 1.00                                  | 1.00                 | 1.00                  | 0.048                    | 0.048               | 1.00                  | 0.068                    | 0.068               |

Figure 9 shows the graphs of  $\bar{f}_{c,v}(\alpha^Q)$  and of  $\bar{E}_{c,v}(\alpha^Q)$  adjusted via Functions (10) and (11), respectively, that best fit the values of the coefficient of variation. Their coefficients of determination ( $R^2$ ) are, respectively, 0.95 and 0.99:

$$\bar{f}_{c,v}(\alpha^Q) = 0.055\alpha^Q^{-1.234} \tag{10}$$

$$\bar{E}_{c,v}(\alpha^Q) = 0.063\alpha^Q^{-1.908} \tag{11}$$

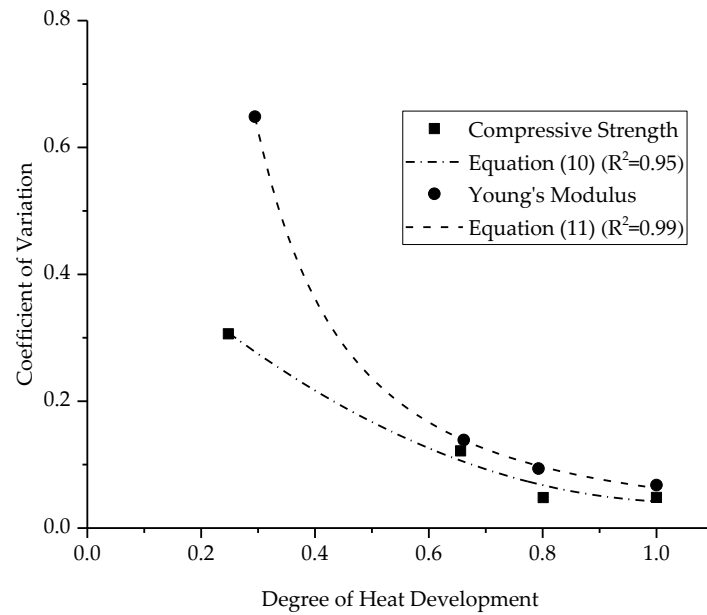


Figure 9. Evolution of the coefficients of variation  $\bar{f}_{c,v}$  and  $\bar{E}_{c,v}$  with  $\alpha^Q$ .

As expected, the heterogeneity of the initial stages of the modulus of elasticity was higher than that of the compressive strength, possibly attributed to the challenges encountered during the test, particularly concerning the positioning and sensitivity of the sensors.

#### 4.4. Statistical Analysis of Flexural Tensile Strength

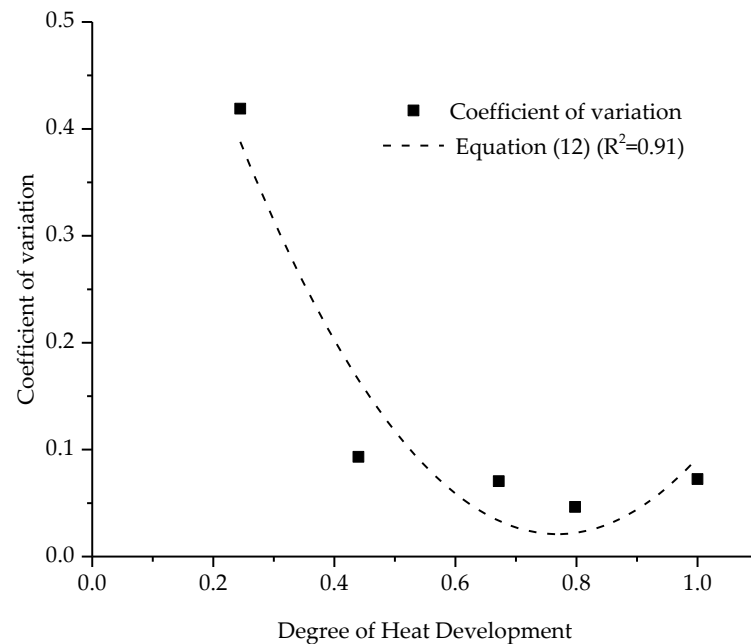
The samples were gathered for the analysis of the flexural tensile strength within 5 clusters, as presented in Table 5, which also provides the principal statistical indicators. Similar to the compressive tests, the coefficient of variation, in contrast to the standard deviation, was higher for the lower degrees of heat development.

Table 5. Results for tensile flexural strength.

| $cl_{kcl}$ | $\alpha^Q_{kcl,inf} - \alpha^Q_{kcl,sup}$ | $\alpha^Q_{kcl,\mu}$ | $\bar{f}_{t,kcl,\mu}$ | $\bar{f}_{t,kcl,\sigma}$ | $\bar{f}_{t,kcl,v}$ |
|------------|---|----------------------|-----------------------|--------------------------|---------------------|
| 1          | 0.15 – 0.35                               | 0.24                 | 0.07                  | 0.030                    | 0.419               |
| 2          | 0.40 – 0.50                               | 0.44                 | 0.27                  | 0.026                    | 0.093               |
| 3          | 0.60 – 0.70                               | 0.67                 | 0.61                  | 0.043                    | 0.071               |
| 4          | 0.75 – 0.85                               | 0.80                 | 0.78                  | 0.036                    | 0.046               |
| 5          | 1.00                                      | 1.00                 | 1.00                  | 0.073                    | 0.073               |

Figure 10 shows the graph of  $\bar{f}_{t,v}(\alpha^Q)$  adjusted via parabolic Function (12), which fits the values of the dispersion coefficient ( $R^2 = 0.91$ ), focusing on increasing these values at the end of the curve:

$$\bar{f}_{t,v}(\alpha^Q) = 1.336\alpha^2 + 2.054\alpha + 0.810 \quad (12)$$



**Figure 10.** Evolution of the dispersion coefficient  $\bar{f}_{t,v}$  with  $\alpha^Q$ .

When we closely observe the experimental results, we see that, for  $\alpha^Q > 0.8$ :

$\bar{E}_{c,v}$  continues to decrease;  
 $\bar{f}_{c,v}$  remains almost constant;  
 $\bar{f}_{t,v}$  increases.

This is due to the existence of diffuse microcracks in the cement paste for this threshold value of 0.8. This diffuse microcracking, which contributes to the heterogeneity within the cement paste, is closely linked to the self-desiccation shrinkage of the paste surrounding the aggregates. While this microcracking has minimal effect or negligible impact on the heterogeneity of the Young's modulus (E) and its temporal evolution associated with the formation of new hydrates, it significantly influences the tensile cracking process of the paste. The heterogeneity induced by this diffuse microcracking has a more pronounced effect than the homogenization resulting from the ongoing hydration process. For this reason, the values of  $\bar{f}_{t,v}$  were adjusted by the parabolic function given in Equation (12).

## 5. Concluding Remarks

This paper presents experimental research that aims to establish a connection between the heterogeneity of mechanical properties and the progression of the hydration reaction. It is essential to emphasize that previous research [38] on the heterogeneity of concretes has indicated that for standard tests conducted appropriately, the variability is not notably significant in comparison to the material's inherent heterogeneity.

The main finding of the present research lies in the observed trend of the coefficient of variation of the mechanical parameters under study (compressive strength, Young's modulus, and tensile strength) with respect to hydration. The alterations in these statistical measures in conjunction with the progression of hydration support the intuition that the material at an early age exhibits a more heterogeneous structure characterized by a higher content of non-hydrated cement and free water.

Nevertheless, upon reaching a particular threshold of hydration (in this case characterized by  $\alpha^Q = 0.8$ ), the heterogeneity linked to the studied properties demonstrated distinct behaviors. This disparity arose due to microcracking and its varied impact on the mechanical properties.

The functions proposed for the evolution of heterogeneity with hydration are not intended to be universally applicable, and the authors acknowledge that a more extensive dataset is required to establish predictive models for the random behavior of concrete of an early age. Nevertheless, these functions are a first attempt to establish formulas that can help the modeling of concrete when probabilistic models are used to consider the scattering of its mechanical properties from an early age.

The probabilistic model on which this research is focused does not directly depend on the microstructural characteristics of the material. It primarily relies on relationships between the volume of specimens and the size of aggregates, a relationship that translates, in terms of numerical modeling, into relationships between the volume of finite elements and the maximum diameter of aggregates. Therefore, the future development of this research will be directed towards specimens and aggregates of different sizes, aiming at the determination of formulas that cover a larger number of concrete types. The four-point bending tests as well as the splitting test provide indirect values of tensile strength. However, such tests, especially the bending test, allow easier manipulation for conducting tests at early ages corresponding to lower degrees of hydration. A possible extension of this research could therefore be the performance of direct tension tests to confirm the results obtained here.

**Author Contributions:** Conceptualization, E.M.R.F. and P.R.; Methodology, R.D.T.F. and P.R.; Formal analysis, G.C.M. and E.M.R.F.; Investigation, G.C.M.; Resources, R.D.T.F.; Writing—original draft, G.C.M.; Supervision, E.M.R.F. All authors have read and agreed to the published version of the manuscript.

**Funding:** This study was financed in part by the Brazilian Agency Coordenação de Aperfeiçoamento de Pessoal de Nível Superior (CAPES)—Finance Code 001.

**Data Availability Statement:** Data are contained within the article.

**Acknowledgments:** The support of Brazilian agencies Conselho Nacional de Desenvolvimento Científico e Tecnológico (CNPq) and Fundação de Amparo à Pesquisa do Estado do Rio de Janeiro (FAPERJ) are gratefully acknowledged.

**Conflicts of Interest:** The authors declare no conflicts of interest.

## References

1. Shinozuka, M. Probabilistic Modelling of Concrete Structures. *J. Eng. Mech.* **1972**, *98*, 1433–1451.
2. Van Mier, J.G.M.; Van Vliet, M.R.A.; Wang, T.K. Fracture Mechanisms in Particle Composites: Statistical Aspects in Lattice Type Analysis. *Mech. Mater.* **2002**, *34*, 705–724. [[CrossRef](#)]
3. Benkemoun, N.; Hautefeuille, M.; Colliat, J.-B.; Ibrahimbegovic, A. Failure of Heterogeneous Materials: 3D Meso-Scale FE Models with Embedded Discontinuities. *Int. J. Numer. Methods Eng.* **2010**, *82*, 1671–1688. [[CrossRef](#)]
4. Tang, X.; Zhou, Y.; Zhang, C.; Asce, M.; Shi, J. Study on the Heterogeneity of Concrete and Its Failure Behavior Using the Equivalent Probabilistic Model. *J. Mater. Civ. Eng.* **2011**, *23*, 402–413. [[CrossRef](#)]
5. Sellier, A.; Millard, A. Weakest Link and Localisation  $WL^2$ : A Method to Conciliate Probabilistic and Energetic Scale Effects in Numerical Models. *Eur. J. Environ. Civ. Eng.* **2014**, *18*, 1177–1191. [[CrossRef](#)]
6. Rossi, P.; Richer, S. Numerical Modelling of Concrete Cracking Based on a Stochastic Approach. *Mater. Struct.* **1987**, *20*, 334–337. [[CrossRef](#)]
7. Tailhan, J.L.; Pont, S.D.; Rossi, P. From Local to Global Probabilistic Modeling of Concrete Cracking. *Ann. Solid Struct. Mech.* **2010**, *1*, 103–115. [[CrossRef](#)]
8. Phan, T.S.; Tailhan, J.-L.; Rossi, P. 3D Numerical Modelling of Concrete Structural Element Reinforced with Ribbed Flat Steel Rebars. *Struct. Concr.* **2013**, *14*, 378–388. [[CrossRef](#)]
9. Rossi, P.; Tailhan, J.-L. Numerical Modeling of the Cracking Behavior of a Steel Fiber-Reinforced Concrete Beam on Grade. *Struct. Concr.* **2017**, *18*, 571–576. [[CrossRef](#)]
10. Rastiello, G.; Tailhan, J.L.; Rossi, P.; Dal Pont, S. Macroscopic Probabilistic Cracking Approach for the Numerical Modelling of Fluid Leakage in Concrete. *Ann. Solid Struct. Mech.* **2015**, *7*, 1–16. [[CrossRef](#)]

11. Rossi, P.; Daviau-Desnoyers, D.; Tailhan, J.L. Probabilistic Numerical Model of Cracking in Ultra-High Performance Fibre Reinforced Concrete (UHPFRC) Beams Subjected to Shear Loading. *Cem. Concr. Compos.* **2018**, *90*, 119–125. [[CrossRef](#)]
12. Mota, M.T.; Fairbairn, M.R.E.; Ribeiro, L.B.F.; Rossi, P.; Tailhan, J.-L.; Andrade, H.C.C.; Rita, M.R. A 3D Probabilistic Model for Explicit Cracking of Concrete. *Comput. Concr.* **2021**, *27*, 549–562. [[CrossRef](#)]
13. Fairbairn, E.M.R.; Ebecken, N.F.F.; Paz, C.N.M.; Ulm, F.J. Determination of Probabilistic Parameters of Concrete: Solving the Inverse Problem by Using Artificial Neural Networks. *Comput. Struct.* **2000**, *78*, 497–503. [[CrossRef](#)]
14. Rossi, P.; Tailhan, J.-L. *Numerical Modeling Strategies for Sustainable Concrete Structures*; RILEM Bookseries; Springer International Publishing: Cham, Switzerland, 2023; Volume 38, ISBN 978-3-031-07745-6.
15. Rossi, P.; Wu, X.; Le Maou, F.; Belloc, A. Scale Effect on Concrete in Tension. *Mater. Struct.* **1994**, *27*, 437–444. [[CrossRef](#)]
16. Fairbairn, E.M.R.; Azenha, M. (Eds.) *Thermal Cracking of Massive Concrete Structures*; RILEM State-of-the-Art Reports; Springer International Publishing: Cham, Switzerland, 2019; Volume 27, ISBN 978-3-319-76616-4.
17. Bažant, Z.P.; Kazemi, M.T. Size Dependence of Concrete Fracture Energy Determined by RILEM Work-of-Fracture Method. *Int. J. Fract.* **1991**, *51*, 121–138. [[CrossRef](#)]
18. Wittmann, F.H.; Mihashi, H.; Nomura, N. Size Effect on Fracture Energy of Concrete. *Eng. Fract. Mech.* **1990**, *35*, 107–115. [[CrossRef](#)]
19. De Schutter, G.; Taerwe, L. Degree of Hydration-Based Description of Mechanical Properties of Early Age Concrete. *Mater. Struct. Mater. Et. Constr.* **1996**, *29*, 335–344. [[CrossRef](#)]
20. Bassam, S.A.; Yu, B.-J.; Ansari, F. Fracture Energy of Concrete by Maturity Method. *ACI Mater. J.* **2007**, *104*, 77–85. [[CrossRef](#)]
21. Kim, J.-K.; Lee, Y.; Yi, S.-T. Fracture Characteristics of Concrete at Early Ages. *Cem. Concr. Res.* **2004**, *34*, 507–519. [[CrossRef](#)]
22. Kolani, B.; Buffo, L.; Sellier, A.; Boutillon, L.; Linger, L. Crack Initiation and Propagation at Early Age. In Proceedings of the Concrete Engineering for excellence and efficiency—10th Fib Symposium Proceedings, Prague, Czech Republic, 8–10 June 2011.
23. Baron, J.; Byfors, J. Properties of Set Concrete at Early Ages State-of-the-Art-Report. *Matériaux Et. Constr.* **1981**, *14*, 399–450. [[CrossRef](#)]
24. Krauß, M.; Hariri, K. Determination of Initial Degree of Hydration for Improvement of Early-Age Properties of Concrete Using Ultrasonic Wave Propagation. *Cem. Concr. Compos.* **2006**, *28*, 299–306. [[CrossRef](#)]
25. Associação Brasileira de Normas Técnicas (ABNT). *NBR 16697: Cimento Portland—Requisitos*; ABNT: Rio de Janeiro, Brazil, 2018.
26. Associação Brasileira de Normas Técnicas (ABNT). *NBR 16605: Cimento Portland e Outros Materiais Em Pó—Determinação da Massa Específica*; ABNT: Rio de Janeiro, Brazil, 2017.
27. Associação Brasileira de Normas Técnicas (ABNT). *NBR 7215—Cimento Portland—Resistência a Compressão*; ABNT: Rio de Janeiro, Brazil, 1996.
28. Larrard, F. *de Concrete Mixture Proportioning: A Scientific Approach*; E & FN Spon: London, UK, 1999; Volume 9, ISBN 9788578110796.
29. Associação Brasileira de Normas Técnicas (ABNT). *NBR NM 52: Agregados Miúdo—Determinação da Massa Específica e Massa Específica Aparente*; ABNT: Rio de Janeiro, Brazil, 2003.
30. Associação Brasileira de Normas Técnicas (ABNT). *NBR NM 53: Agregado Graúdo—Determinação de Massa Específica, Massa Específica Aparente e Absorção de Água*; ABNT: Rio de Janeiro, Brazil, 2009.
31. Associação Brasileira de Normas Técnicas (ABNT). *NBR NM 30 Agregado Miúdo—Determinação Da Absorção de Água*; ABNT: Rio de Janeiro, Brazil, 2001.
32. Associação Brasileira de Normas Técnicas (ABNT). *NBR NM 248 Agregados—Determinação Da Composição Granulométrica*; ABNT: Rio de Janeiro, Brazil, 2003.
33. De Larrard, F.; Sedran, T. A New Approach for the Formulation of Concrete. *Ann. du Bâtiment des Trav. Publics* **1999**, *6*, 39–54.
34. Byfors, J. *Plain Concrete At Early Ages*; Swedish Cement and Concrete Research Institute: Stockholm, Sweden, 1980.
35. Rocha, C.A.A. Influência Da Pressão e Temperatura de Cura e Da Adição de NaCl e KCl No Comportamento de Pastas Para Cimentação de Poços de Petróleo. Ph.D. Thesis, Federal University of Rio de Janeiro, Rio de Janeiro, Brazil, 2015.
36. Klemczak, B.; Batog, M.; Pilch, M. Assessment of Concrete Strength Development Models with Regard to Concretes with Low Clinker Cements. *Arch. Civ. Mech. Eng.* **2016**, *16*, 235–247. [[CrossRef](#)]
37. Fairbairn, E.M.R.; Ferreira, I.A.; Cordeiro, G.C.; Silvano, M.M.; Filho, R.D.T.; Ribeiro, F.L.B. Numerical Simulation of Dam Construction Using Low-CO<sub>2</sub>-Emission Concrete. *Mater. Struct. Mater. Et. Constr.* **2010**, *43*, 1061–1074. [[CrossRef](#)]
38. Rossi, P.; Ulm, F.-J.; Hachi, F. Compressive Behavior of Concrete: Physical Mechanisms and Modeling. *J. Eng. Mech.* **1996**, *122*, 1038. [[CrossRef](#)]

**Disclaimer/Publisher’s Note:** The statements, opinions and data contained in all publications are solely those of the individual author(s) and contributor(s) and not of MDPI and/or the editor(s). MDPI and/or the editor(s) disclaim responsibility for any injury to people or property resulting from any ideas, methods, instructions or products referred to in the content.